Eur Biophys J (1993) 22:225–236

European Biophysics Journal

The molecular force field of guanine and its deuterated species as determined from neutron inelastic scattering and resonance Raman measurements

Z. Dhaouadi [1], M. Ghomi [1], Ce. Coulombeau [2], C. Coulombeau [2], H. Jobic [3], P. Mojzes [4,*], L. Chinsky [4], P. Y. Turpin [4]

[1] Physique Théorique des Macromolécules Biologiques, UFR Santé-Médecine-Biologie Humaine, Université Paris XIII, 74 rue Marcel Cachin, F-93012 Bobigny Cedes, France
[2] Laboratoire d'Etudes Dynamiques et Structurales de la Sélectivité, CNRS URA 332, Université Joseph Fourier, B.P 53X, F-38041 Grenoble Cedex, France
[3] Institut de Recherche sur la Catalyse, 2 avenue Albert Einstein, F-69626 Villeurbanne Cedex, France
[4] Laboratoire de Physique et Chimie Biomoléculaires, CNRS URA 198, Institut Curie et Université Paris VI, 11 rue Pierre et Marie Curie, F-75231 Paris Cedex 05, France

Received: 8 March 1993 / Accepted in revised form: 20 May 1993

Abstract. Neutron inelastic scattering (NIS) spectra from polycrystalline samples and ultraviolet resonance Raman scattering (RRS) spectra from aqueous solutions of guanine and C8-deuterated and (N9, N1, C2-amino)-deuterated guanine are reported. These measurements allowed theoretical simulations of the vibrational wavenumbers and intensities of the NIS and RRS bands to be performed. A valence force field enabled the normal mode wavenumbers, as well as the atomic displacements, to be calculated. The NIS intensities were simulated by considering multi-phonon interactions arising from the lattice mode couplings with the internal molecular vibrational modes. The RRS intensities were simulated within the framework of the so-called "small shift approximation", by using the molecular bond-order changes induced by the electronic transition from the ground to the first electronic excited state. It is shown that NIS spectroscopy mainly provides information on the guanine out-of-plane modes of vibration, while RRS allows the in-plane stretching vibrational motions to be analyzed.

Key words: Resonance Raman spectroscopy – Neutron inelastic scattering – Vibrational spectroscopy – Guanine – Nucleic acids

I. Introduction

Recently, a neutron inelastic scattering (NIS) spectrum of a low-temperature polycrystalline guanine sample (native species) was reported (Coulombeau et al. 1991). The normal mode wavenumbers were calculated using an already existing in-plane force field (Majoube 1984) and a new out-of-plane force field, along with a one-phonon (first-order) NIS intensity simulation, in the 150–1800 cm^{-1} spectral region. This preliminary investigation showed that the external- (lattice modes) and molecular internal vibrational modes of guanine are located in two distinct spectral regions. Since the spectral features below 150 cm^{-1} are mainly constituted by the lattice modes, the couplings between the internal and external modes were neglected in this first paper.

In the present work, we report new results on the low-temperature NIS spectra from polycrystalline deuterated guanine species. Although the NIS technique is a powerful tool for the analysis of the low-wavenumber modes, located below 1000 cm^{-1} and assigned to the base out-of-plane vibrations, the NIS intensities decrease considerably above 1000 cm^{-1} (owing to reduced statistics arising from a considerable decrease of scattered neutron flux, as well as to an additional instrument effect in this spectral region) where the base in-plane modes of vibration contribute. Thus we also report here the UV-resonance Raman scattering (RRS) spectra obtained from aqueous solutions of the native and deuterated compounds, because RRS spectroscopy enables the in-plane modes of vibration to be studied, especially those arising from double-bond stretching motions (principally located above 1000 cm^{-1}). In doing this, we show the complementary capabilities of RRS and NIS measurements for obtaining a reliable force field for the nucleic acid bases. A complete force field can be obtained from the simultaneous analysis of the RRS and NIS spectra, owing to their ability to account for the observed spectral features in both the high- and low-wavenumber vibrational regions.

The main reasons for using the present methodology are related to the fact that the assignments of the vibrational modes based only on classical methods such as IR absorption and/or off-resonance Raman spectroscopies

* *Permanent address*: Institute of Physics of Charles University, Ke Karlovu 5, 12116 Prague 2, Czech Republic
Correspondence to: M. Ghomi

often lead to somewhat inaccurate results. The valance force field based on the joint use of the NIS and RRS data enables a better assignment of the molecular vibrational modes to be obtained, reproducing the vibrational wavenumbers (and their shifts upon selective deuterations) and NIS band intensities. In addition, the RRS spectral intensities can also be simulated, provided that the molecular bond-order changes induced by the transition from the ground to the electronic excited state are known. This theoretical procedure accounts for a higher proportion of the experimental data and consequently decreases the uncertainty in the determination of the force constant values, whose number is always greater than that of the observed wavenumbers.

In addition to the NIS first-order spectral intensity simulation, we also attempted to study the couplings between the external (lattice-modes) and internal molecular modes observed in the NIS spectra. As will be shown, this coupling gives rise to broadening of the first-order NIS bands and to an increase of the spectral background. To reproduce these effects in our simulation, we have taken into account the additive combinations of the internal molecular modes with the external modes, up to the third-order.

II. Experimental methods and results

In the following, we describe two different experimental methods to prepare samples for NIS and RRS measurements. In fact, there is a considerable difference in the amount of sample needed for these two experimental approaches. The amount required for RRS measurements is low (10^{-4} M in 1 ml), while, owing to the weak scattered neutron flux, a substantial amount of crystalline powder (1–3 g) is necessary for the NIS measurements.

A. Sample preparation and NIS measurements

The guanine base (Fig. 1) was purchased from Aldrich and was used as supplied. The guanine deuterated species, hereafter designated as: G-d5 (N1-, N9-, C8- and C2-amino-deuterated guanine), G-d4 (N1-, N9- and C2-amino-deuterated guanine) and G-d1 (C8-deuterated guanine) were prepared from guanine by deuterium substitution (Delabar and Majoube 1978), in the following manner:

– G-d5 was obtained by dissolving and heating up to 100 °C for four hours, 3 g of guanine base in 85 ml of 1 N, $NaOD/D_2O$ solution. After cooling, the solution was neutralized at pD7 by a 10 N D_2SO_4/D_2O solution to precipitate G-d5.

– G-d4 was obtained by dissolving and heating up to 100 °C for six hours, 3 g of guanine base in 100 ml of 1 N D_2SO_4/D_2O solution. A long time is needed to get complete dissolution of guanine. After cooling, the solution was neutralized at pD7 by a 10 N $NaOD/D_2O$ solution to precipitate G-d4.

– G-d1 was obtained by dissolving and heating up to 100 °C for six hours, 3 g of G-d5 in 100 ml of 1 N H_2SO_4/H_2O solution. After cooling, the solution was neutralized at pH 5 by a 2 N $NaOH/H_2O$ solution to precipitate G-d1.

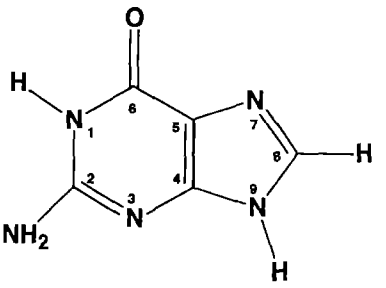

Fig. 1. Chemical structure and atom numbering of the guanine molecule

The isotopic purity of the NIS samples was checked by mass spectroscopy. The mass spectra indicated that the average valus of deuteration were 79%, 81% and 83% for the G-d5, G-d4 and G-d1 species, respectively.

The NIS spectra of guanine and its deuterated derivatives (G-d1 and G-d4) were obtained at the Rutherford Appleton Laboratory, UK. The technical details of the experimental apparatus have been described elsewhere (Penfold and Tomkinson 1988). The NIS spectra were recorded from the polycrystalline powder of each compound at low temperature ($T = 10$ K) in order to sharpen the fundamental lines by decreasing the Debye-Waller factor (Jobic and Lauter 1988).

Traces a, b and c of Fig. 2 show the NIS spectra of guanine, G-d1 and G-d4 in the spectral region below 1800 cm^{-1}. On the basis of a previous normal coordinate analysis (Coulombeau et al. 1991), we have shown that the lattice modes of guanine (external modes) are located below 150 cm^{-1}. Thus, all of the NIS bands located in the 150–1800 cm^{-1} can be assigned to the internal molecular modes and their combinations with the lattice modes. This will also be confirmed by the present normal mode analysis.

B. Sample preparation and RRS measurements

Because the solubility of guanine in water is low, its Raman spectrum in aqueous solution has never been published. However, through heating and vortexing the aqueous solutions, the solubility becomes sufficient for resonance Raman measurements (with multiscans) in a 10^{-2} M phosphate buffer, pH 7. The C8-deuterium substitution was obtained by heating a guanine D_2O solution at 80 °C for two hours, and recrystallizing from H_2O. This sample (G-d1) was then redissolved in an aqueous phosphate buffer for Raman measurements. The G-d4 species was prepared by dissolving the guanine base in a D_2O phosphate buffer at pD7.

In all cases, it was necessary to subtract the appropriate buffer contribution in the O–H (O–D) bending region, by taking as intensity standard the O–H (O–D) stretching bands. The resonance Raman spectra of the

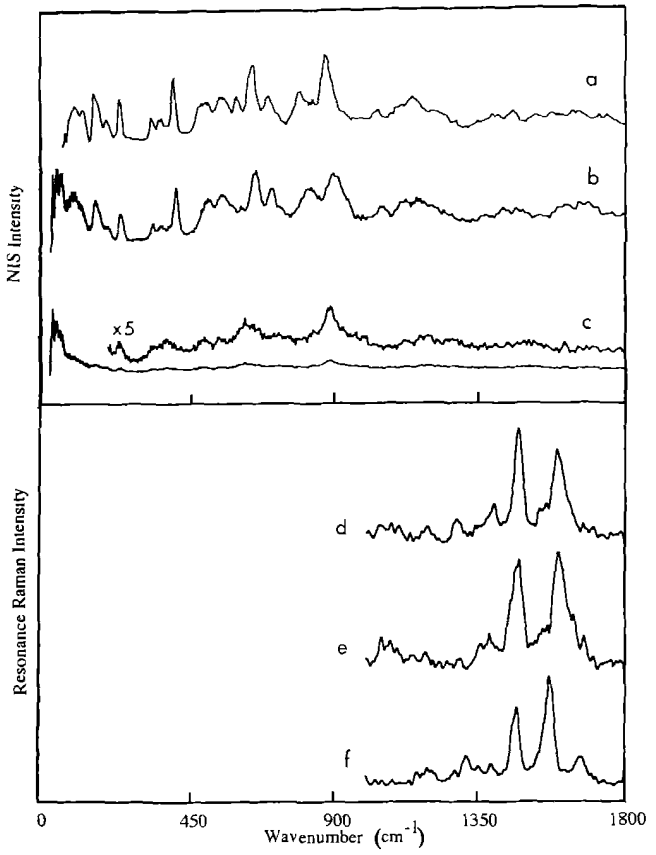

Fig. 2. NIS spectra of guanine *a*, G-d1 *b* and G-d4 *c* species, observed from a polycrystalline sample at $T = 10$ K, and RRS spectra of the same species (guanine *d*, G-d1 *e* and G-d4 *f* observed in aqueous solutions at room temperature with the 257 nm excitation wavelength

various solutions of guanine and its deuterated species were recorded using a 257 nm excitation wavelength, as described before (Dhaouadi et al. 1993). Traces d, e and f of Fig. 2 show the RRS spectra of the native guanine, G-d1 and G-d4 species in the spectral region above 1000 cm^{-1}. Below 1000 cm^{-1}, the RRS information content is rather low and is hampered by a poor signal/noise ratio. The strong and well resolved Raman peaks detected above 1000 cm^{-1}, where the NIS spectra provide only broad and weak bands, confirm the complementary merits of the NIS and RRS techniques as regards the vibrational mode analysis of this nucleic base.

III. Theoretical methods and results

The vibrational mode wavenumbers and the atomic displacements were computed using a home-made calculation code (BORNS) developed within the framework of the Wilson GF-method (Wilson et al. 1955). The redundant internal coordinates were removed by a diagonalization procedure of the G-matrix (Gusoni and Zerbi 1968). The normalized atomic displacement amplitudes derived from this calculation were further employed in our NIS intensity simulations (Brunel et al. 1985; Jobic and Lauter 1988; Dhaouadi et al. 1993). The additional input of the bond-order changes was necessary for simulating the RRS intensities.

A. Empirical valence force field

The guanine base and its deuterated species (G-d1 and G-d4) are supposed to be planar (Cs symmetry). Thus, 42 vibrational modes can be expected from these molecules, of which 29 are in-plane (A′-symmetry) and 13 out-of-plane (A″-symmetry). All of these modes are considered in the present calculations.

In the present paper, the out-of-plane valence force constants of guanine reported in our previous paper (Coulombeau et al. 1991) have been used as input parameters. Only slight changes have been made in the interaction force constants (non-diagonal terms): this was sufficient to successfully reproduce the NIS band shifts and intensities observed upon selective deuteration of the guanine molecule.

The in-plane force field we used in our previous work was that proposed by Majoube (1984). In the present work we found that only slight modifications in the non-diagonal terms of this force field allowed the NIS and RRS isotopic shifts and intensities for the whole set of spectra to be very well reproduced.

Table 1 shows the values of all of the force constants introduced in our present calculations. It should be mentioned that, to limit their number, only the force constants of interaction between adjacent internal coordinates have been considered. The simulation of 104 experimental wavenumbers and 65 NIS and RRS band intensities, from guanine and its deuterated species (Tables 2–5), has been carried out by using 143 force constants and 12 bond-order changes (Tsuboi et al. 1987) (see Sect. C for details). The refinement of the interaction force constants has been carried out by using a least squares method. For a given vibrational mode, the square of the difference between the experimental and calculated wavenumbers has been weighted by the square of the difference between the experimental and calculated intensities of the same mode, for all of the NIS and RRS spectra.

B. Calculated wavenumbers and assignments

The calculated wavenumbers of the in-plane modes, as well as their assignments based on the Potential Energy Distribution (PED) matrix, are given in the Tables 2, 3 and 4 for guanine, G-d1 and G-d4 species, respectively. In these tables we also give the vibrational wavenumbers obtained from IR and off-resonance Raman measurements of polycrystalline samples (Majoube 1984). Table 5 contains the calculated and NIS results for the out-of-plane vibrational modes.

C. NIS and RRS intensity simulations

For simulating the NIS and RRS intensities we have used the theoretical formalisms and the mathematical expres-

Table 1. Valence force constants for guanine in-plane and out-of-plane modes

In-Plane force constants				Out-of-plane force constants			
Diagonal		N7C5, C8N7	0.69	Diagonal		Torsion-Torsion	
		N7C5, C4C5	0.68				
K(N9–H)	4.710	C4C5, C4N9	0.55	W(C8–H)	0.32	TO(C4N9), TO(N9C8)	0.15
K(N9–C8)	6.220	C2N3, N3C4	0.99	W(N9–H)	0.34	TO(C4N9), TO(C8N7)	−0.05
K(N1–C6)	5.590	C2N3, C2N1	0.99	W(N1–H)	0.35	TO(C4C5), TO(N3C4)	−0.3
K(C2–N2)	7.240	C5C4, C5C6	0.85	W(NH2)	0.048	TO(C5C6), TO(C2N1)	−0.18
K(N7=C8)	7.550	C5C4, C4N3	0.85	W(C=O)	0.45	TO(C2N2), TO(C2N3)	−0.15
K(C2=N3)	7.600	C5C4, C2N3	0.6	W(C2–N2)	0.43	TO(C2N2), TO(C2N1)	0.03
K(C=O)	9.810	C5C4, C8N7	−0.1	TO(C–N) (im)	0.49	TO(N9C8), TO(C8N7)	0.18
K(C=C)	6.600			TO(C=N) (im)	0.57	TO(C8N7), TO(N7C5)	0.2
K(C–C)	6.410	Bend-Bend		TO(C=C)	0.52	TO(N7C5), TO(C4C5)	0.25
K(N1–H)	4.070			TO(C–N) (py)	0.32	TO(C4C5), TO(C4N9)	0.3
K(C8–H)	5.360	HNH, CN2H	−0.013	TO(C=N) (py)	0.629	TO(C2N1), TO(C2N3)	−0.1
K(N2–H)	5.840	CN2H, N3C2N2	−0.05	TO(C–C) (py)	0.52	TO(C2N1), TO(N1C6)	−0.25
K(N7–C5)	5.500	CN2H, N1C2N2	−0.05	TO(C2–N2)	0.08	TO(N1C6), TO(C5C6)	−0.25
K(N9–C4)	6.400	C4N9H, C4N9C8	0.45			TO(C5C6), TO(C4C5)	−0.25
K(N1–C2)	6.310	C8N9H, C4N9C8	0.45	Wag-Wag		TO(N9C8), TO(N7C5)	0.1
K(N3–C4)	6.480	C6N1H, C6N1C2	0.1			TO(C8N7), TO(C4C5)	0.05
H(N3C4N9)	1.460	C2N1H, C6N1C2	0.1	W(NH2), W(C2N2)	0.007	TO(N9C8), TO(C4C5)	−0.05
H(N3C2N2)	1.700			W(C8H), W(N9H)	−0.03	TO(C4N9), TO(N7C5)	0.02
H(N1C2N2)	1.720	Stretch-Bend		W(C8H), W(N1H)	0.03	TO(N1C6), TO(C2N3)	−0.13
H(N7C8N9)	1.940			W(N1–H), W(C2–N2)	−0.16	TO(N1C6), TO(C4C5)	−0.13
H(N3C2N1)	1.960	C=O, C5C=O	0.9			TO(C2N3), TO(C4C5)	−0.1
H(N–C=O)	1.256	C=O, N1C=O	0.9	Wag-Torsion		TO(N3C4), TO(C2N1)	−0.05
H(C–C=O)	0.672	C8N9, C8N9H	0.1			TO(N3C4), TO(C5C6)	−0.07
H(N7–CC)	0.940	N3C4, C4N3C2	0.99	W(N9–H), TO(N9C8)	−0.095		
H(N1–CC)	1.570	N9C8, N7C8N9	−0.3	W(C8–H), TO(N9C8)	0.08		
H(C–C=C)	1.370	N9C8, C8N9C4	−0.3	W(C=O), TO(C6N1)	0.05		
H(N–C–H)	0.420	C5C6, C5C=O	0.300	W(N1–H), TO(N1C2)	0.24		
H(N=C–H)	0.423	N1C6, N1C=O	0.500	W(C2–N2), TO(C2N3)	−0.037		
H(C–N1–H)	0.380	C8N9, N9C8H	0.990	W(C2–N2), TO(C2N2)	−0.03		
H(C–N2–H)	0.641	C8N7, N7C8H	0.45	W(N9–H), TO(N9C4)	0.13		
H(H–N–H)	0.432	C6N1, C6N1H	−0.07	W(C8–H), TO(C8N7)	−0.13		
H(C8N9C4)	1.480	C2N2, CNH	0.35	W(C=O), TO(C6C5)	0.35		
H(C6N1C2)	1.180	N7C5, C8N7C5	−0.05	W(N1–H), TO(N1C6)	−0.14		
H(C–N9–H)	0.389	N7C5, N7C5C4	−0.05	W(C2–N2), TO(C2N1)	0.02		
H(C5N7C8)	1.580	C4N9, C4N9C8	0 67				
H(C4N3C2)	2.250	C8N7, C8N7C5	−0.6				
H(N3C4C5)	1.260	C8N7, N9C8N7	−0.6				
H(N9C4C5)	1.270	C5C4, C5C4N9	0.45				
H(N7C5C4)	1.000	C5C4, N7C5C4	0.45				
		N1C2, N1C2N3	0.97				
Stretch-Stretch		N1C2, C6N1C2	0.97				
		C2N3, C2N3C4	0.99				
N9C8, N9C4	0.99	C2N3, N3C2N1	0.99				
C=O, C5C6	0.6	C6N1, C6N1C2	0.99				
C=O, N1C6	0.6	C6N1, N1C6C5	0.99				
C6N1, N1C2	0.75	C5C6, N1C6C5	0.99				
C6N1, C5C6	0.75	C5C6, C6C5C4	0.99				
C2N2, C2N1	0.45	C5C4, N3C4C5	0.35				
C2N2, C2N3	0.45	C5C4, C6C5C4	0.35				
N9C8, C8N7	0.9						

Symbols: (py) = pyrimidine ring. (im) = imidazole ring. K = stretching force constant (mdyn/Å), H = bending force constant (mdyn · Å). W = wagging force constant, TO = torsional force constant. Units for interaction force constants: Stretch-Stretch force constants (mdyn/Å), Bend-Bend force constants (mdyn · Å), Stretch-Bend force constants (mdyn), Wag-Wag force constants (mdyn · Å), Wag-Torsion force constants (mdyn · Å) and Torsion-Torsion force constants (mdyn · Å). For atom numbering see also Fig. 1

sions described in our previous papers on NIS and RRS spectral analysis (Brunel et al. 1985; Jobic and Lauter 1988; Dhaouadi et al. 1993). Thus, in the present paper, we only mention the main approximations used and we report the corresponding simulated spectra.

The NIS peak intensities for the first-order interactions have been calculated by taking into account all atom (i.e. H, C, N and O) coherent and incoherent contributions. Obviously for the pure species the hydrogen atom incoherent contribution is dominant, owing to its large incoherent cross-section. The calculated first-order intensities arising from internal molecular modes are shown in the lower part of Figs. 3–5 for guanine and its deuterated species.

Table 2. Comparison between experimental and calculated wavenumbers (cm^{-1}) for the guanine in-plane modes. The assignments are based on the internal coordinates for which the potential energy distribution (PED) is reported in % (PED contributions lower than 5% are not reported). IR and R stand for polycrystalline infrared and Raman peaks, respectively (Majoube 1984). The experimental wavenumbers arising from RRS and NIS spectra are also reported. For atom numbering see also Fig. 1

Wavenumber (cm^{-1})					Assignments (PED)
IR	R	RRS	NIS	CALC.	
3316				3309	N–H2 asym. St. (100%)
3180				3199	N–H2 sym. St. (100%)
	3115			3151	C8–H (99%)
2908				2928	N9–H (99%)
2996				2721	N1–H (99%)
1702				1703	C6=O6 (45%); C5–C6 (15%)
				1686	H–N–H (45%); C2N2H (26%); C6=O6 (12%)
1675	1678			1667	C2–N2 (41%); H–N–H (12%); C4N3C2 (7%); N3C2N1 (6%); N1–C2 (4%); C6N6H (5%)
1638		1635	1642	1619	C2=N3 (39%); N1–C2 (15%); N3C2N2 (6%); N1C2N2 (9%)
	1604	1595		1603	N3–C4 (16%); C4–N9 (11%); C6=O6 (8%); C5=C4 (7%); H–N9C4 (7%); H–N9C8 (6%); N9C4=C5 (5%)
1550	1552			1557	N7–C5 (26%); C8=N7 (16%); C5–C6 (10%); C6C5C4 (6%)
				1491	C8=N7 (22%); N9–C8 (16%); C4–N9 (10%); C5=C4 (9%); C8N7C5 (9%); N7–C5 (7%); C6=O6 (6%)
1477	1480	1475		1480	C8=N7 (20%); C5=C4 (18%); C4–N9 (8%); C2–N2 (8%); N3C4N9 (7%); N1–C2 (5%)
1375	1392	1400		1399	N3–C4 (24%); C4–N9 (18%); N9–C8 (15%); C5–C6 (11%); N7–C5 (8%)
1261	1266	1281		1288	C2N1–H (24%); C6N1–H (21%); C6–N1 (18%); C2–N2 (9%); C6=O6 (6%)
1216	1232			1226	N7C8–H (23%); N9C8–H (19%); C6=O6 (13%); C5–C6 (12%); C8N7C5 (6%)
1174	1188	1189	1154	1156	H–N9C8 (40%); H–N9C4 (38%); N9C8–H (5%)
1118			1100	1131	C2N2–H (25%); N7C8–H (15%); N9C8–H (13%); C2=N3 (11%); N9–C8 (8%)
				1081	C2N2–H (21%); N7C8–H (12%); N9C8–H (10%); N9–C8 (8%); C6–N1 (7%); C2=N3 (7%)
1052	1042		1033	1045	C6–N1 (34%); C6N1–H (12%); C2N1–H (7%); C5C6O6 (8%); N1C6O6 (7%); N3–C4 (5%)
950	940			966	N1–C2 (30%); C2=N3 (15%); C2N1–H (10%); C4–N9 (6%)
850	850			865	N9–C8 (26%); N9C8–H (18%); C8N7C5 (7%); N9C8N7 (5%); N7C8–H (5%); C5=C4 (5%)
				791	C2–N2 (19%); C4N9C8 (13%); N7–C5 (11%); N9C8N7 (9%); N9C4C5 (7%); C4N3C2 (6%); N3C2N1 (6%)
726	712		699	702	N1C2N2 (15%); N1C6O6 (14%); N3C2N2 (10%); C5C6O6 (9%)
645	651			664	N1C6C5 (14%); C2–N2 (13%); C4–N9 (8%); C2N1C6 (8%); C6=O6 (7%); N1–C2 (7%); N3–C4 (5%)
557	547		592	577	C4–N9 (21%); N3C4C5 (13%); C2N1C6 (8%); C8N7C5 (6%); C4N3C2 (5%)
516	496			502	N7–C5 (19%); C2–N2 (12%); N3–C4 (7%); C4N3C2 (7%); N1C6C5 (7%); C6C5C4 (6%)
348	343		358	353	N3C2N2 (16%); N1C2N2 (15%); N1–C2 (14%); C6–N1 (11%); N3–C4 (10%); N1C6O6 (6%); C5C6O6 (6%); C2=N3 (5%)
				329	C5C6O6 (17%); C5–C6 (17%); N1C6O6 (14%); N7C5C6 (13%); N3C4N9 (8%); N7C5C4 (5%)

Table 3. Same as Table 2, but for the G-d1 (C8-deuterated guanine) in-plane modes

Wavenumber (cm^{-1})					Assignments (PED)
IR	R	RRS	NIS	CALC.	
3326				3309	N–H2 asym. St. (100%)
3179				3199	N–H2 sym. St. (100%)
2880				2928	N9–H (99%)
2664				2721	N1–H (99%)
2316				2368	C8–D (96%)
1698				1702	C6=O6 (46%); C5–C6 (14%)
1673	1675	1675		1686	H–N–H (45%), C2N2–H (26%); C6=O6 (12%)
1633		1643		1667	C2–N2 (41%); H–N–H (12%); C4N3C2 (7%); N3C2N1 (6%); N1–C2 (6%); C2N2–H (5%)
	1605	1599		1618	C2=N3 (41%); N1–C2 (17%); N1C2N2 (9%); N3C2N2 (6%); C2N2–H (5%)
				1589	N3–C4 (22%); C4–N9 (11%); C5=C4 (11%); N7–C5 (8%); N9C4C5 (7%); H–N9C4 (6%)
1554	1557	1559		1538	N7–C5 (22%); C8=N7 (13%); C5–C6 (11%)
				1477	C4–N9 (18%); C8=N7 (16%); N9–C8 (12%); N7–C5 (9%); C8N7C5 (8%); C5=C4 (7%)
1472		1475		1472	C8=N7 (30%); C5=C4 (14%); C4–N9 (9%); C2–N2 (6%); N3C4N9 (6%)
1360	1360	1356		1361	N9–C8 (25%); N3–C4 (16%); C5–C6 (14%); C4–N9 (8%)
				1283	C2N1–H (26%); C6N1–H (24%); C6–N1 (15%); C6=O6 (11%); C2–N2 (9%)
1200	1211			1180	N3–C4 (14%); H–N9C8 (13%); H–N9C4 (12%); C5–C6 (12%); C6=O6 (11%); C8=N7 (6%)
1125				1139	H–N9C8 (19%); H–N9C4 (17%); C2N2–H (18%); N9–C8 (13%); C2=N3 (10%)
				1097	C2N2–H (36%); C2–N3 (14%); H–N9C8 (9%); H–N9C4 (9%); C6–N1 (5%)
1043	1050		1039	1045	C6–N1 (31%); C6N1–H (12%); C2N1–H (7%); C5C6O6 (8%); N1C6O6 (6%); N3–C4 (6%)
			988	985	N1–C2 (25%); N7C8-D (9%); N9C8–D (6%); C2N1–H (6%); C2=N3 (6%)
944	942		960	930	N7C8–D (20%); N9C8–D (11%); N1–C2 (9%); C2=N3 (9%); C6–N1 (6%); C2–N2 (5%)
838	838		817	814	N9C8–D (41%); N7C8–D (21%); N9–C8 (17%)
				786	C2–N2 (18%); N7–C5 (11%); C4N9C8 (10%); N7C8–D (8%); N9C8N7 (7%); N3C2N1 (7%)
			709	701	N1C2N2 (16%); N1C6O6 (14%); N3C2N2 (10%); C5C6O6 (9%)
645	646		650	661	N1C6C5 (14%); C2–N2 (13%); C2N1C6 (9%); N1–C2 (6%); C6=O6 (6%); C4–N9 (6%)
557	561		546	570	C4–N9 (20%); N3C4C5 (11%); N9C8–D (7%); N7C8–D (6%); C8N7C5 (6%); C2N1C6 (6%)
494	494		498	498	N7–C5 (19%); C2–N2; (11%); N3–C4 (7%); N1C6C5 (7%); C6C5C4 (6%); C4N3C2 (6%)
			355	352	N3C2N2 (16%); N1C2N2 (15%); N1–C2 (14%); C6–N1 (11%); N3–C4 (9%); N1C6O6 (7%)
345	338		331	325	C5–C6 (17%); C5C6O6 (16%); N1C6O6 (13%); N7C5O6 (14%); N3C4N9 (9%); N7C5C4 (6%)

Previously, it has been shown that the higher order NIS spectra can be simulated by computing the convolution products of the first-order spectrum (arising from the internal molecular modes) with the lattice spectrum (Brunel et al. 1985; Jobic and Lauter 1988; Dhaouadi et al. 1993). In the present work, the higher order (up to the third-order) NIS intensities have been simulated. For this multi-phonon simulation, only the additive contributions have been taken into account because at $T = 10$ K, the subtractive contributions are negligible. The different

Table 4. Same as Table 2, but for the G-d4 (N9-, N1- and N2-deuterated guanine) in-plane modes

Wavenumber (cm^{-1})					Assignments (PED)
IR	R	RRS	NIS	CALC.	
3108				3151	C8–H (99%)
2516				2469	N2–D asym. St. (98%)
				2320	N2–D sym. St. (96%)
2114				2169	N9–D (96%)
2070				2014	N1–D (96%)
				1695	C6=O6 (54%); C5–C6 (16%)
1676	1660	1667		1656	C2–N2 (42%); C4N3C2 (10%); N3C2N1 (9%); N1–C2 (8%); C6=O6 (5%); N3C2N2 (5%)
1610	1600			1590	C2=N3 (37%); N1–C2 (11%); N1C2N2 (7%)
1564	1567	1575		1586	N3–C4 (16%); C2=N3 (11%); C4–N9 (9%); N7–C5 (9%); C5=C4 (7%); C6=O6 (6%); C5–C6 (6%); N9C4C5 (6%)
1529	1531			1550	C8=N7 (23%); N7–C5 (20%); C6=O6 (8%); N1–C2 (7%); C5–C6 (6%)
				1486	C8=N7 (25%); N9–C8 (18%); C4–N9 (10%); C8N7C5 (9%); N7–C5 (8%); C6=O6 (5%)
1457	1466	1471		1468	C5=C4 (20%); C8=N7 (14%); C2–N2 (11%); C4–N9 (9%); N1–C2 (6%); N3C4N9 (6%)
1364	1368	1398		1384	N3–C4 (21%); N9–C8 (17%); C4–N9 (17%); C5–C6 (9%); N7–C5 (7%); N9C8–H (6%)
1280	1285			1262	D–N–D (34%); C2N2–D (21%); C6–N1 (10%); C2–N2 (9%)
1250				1230	N7C8–H (24%); N9C8–H (20%); D–N–D (11%); C5–C6 (11%); C6–N1 (7%)
1168				1170	C6–N1 (27%); C6=O6 (18%); N1–C2 (11%); C2N1–D (9%); C6N1–D (7%)
1099				1100	N7C8–H (21%); N9C8–H (18%); N9–C8 (12%)
987	990			1003	C2=N3 (18%); N3–C4 (12%); C4–N9 (9%); C6–N1 (8%); N1C6O6 (6%), N1–C2 (5%)
				944	C2N2–D (17%); C6N1–D (10%); C2N1–D (8%); N1C6O6 (7%); C5C6O6 (6%); C2=N3 (6%)
886			880	873	D–N9C8 (40%); D–N9C4 (37%); N9–C8 (5%)
828	825			851	N9–C8 (22%), N9C8–H (15%); C2N2–D (7%)
817				788	C2N1–D (16%); C6N1–D (11%); C2N2–D (12%); N1–C2 (10%); C4N9C8 (8%); N9C8N7 (8%)
				761	C2–N2 (10%); C2N1–D (9%); C6N1–D (7%); C2N2–D (7%); C4N9C8 (7%); N9C4C5 (6%)
662	652			646	N1C6C5 (15%); C2–N2 (13%); C2N1C6 (9%); C6=O6 (7%); N1–C2 (6%); C4–N9 (6%)
635	640		626	627	C6N1–D (16%); C2N1–D (9%); N1C2N2 (11%); C6–N1 (8%); N1C6O6 (8%); C5C6O6 (7%)
547	551			548	C4–N9 (21%); N3C4C5 (12%); D–N9C4 (7%); N3C4N9 (5%); C2N1C6 (5%)
500	489			490	N7–C5 (17%); C2–N2 (13%), N3–C4 (8%), C4N3C2 (7%); N1C6C5 (6%); C6C5C4 (5%)
				331	C5C6O6 (21%); N1C6O6 (18%); N1–C2 (13%); C5–C6 (9%); N3C2N2 (8%); N1C2N2 (7%)
337	340			320	N3–C4 (11%); N3C4N9 (11%); N3C2N2 (10%); N1C2N2 (9%); N7C5C6 (10%); C5–C6 (8%)

steps of the NIS spectral simulation (in the case of pure guanine) are shown in Fig. 6. The spectral shape of the first-order spectrum (Fig. 6a) was simulated by Gaussians whose maximum intensities are shown in the lower part of Fig. 3. In order to account for the experimental resolution, which decreases rapidly in the high-wavenumber region of the NIS spectra (above 1000 cm^{-1}), the half-width of the NIS Gaussian bands has been assumed to be a quadratic function of the spectral wavenumber. The second-order spectrum was evaluated by convolving the

Table 5. Calculated wavenumbers (cm^{-1}) for the guanine out-of-plane modes. The assignments are based on the internal coordinates for which the potential energy distribution (PED) is reported in % (PED contributions lower than 5% are not reported). In front of each calculated wavenumber, the first number in parentheses represents the shift observed upon C8-deuteration (G-d1 species), while the second number corresponds to that observed upon deuteration at the N9, N1 and N2 atoms (G-d4 species). W and TO stand for wagging and torsion internal coordinates, respectively. For atom numbering see also Fig. 1

Wavenumber (cm^{-1})		Assignments (PED)
NIS	CALC.	
	921 (−2, −193)	W(N9H) (38%); TO(N9C8) (17%); W(C8H) (13%); W(C2N2) (10%); TO(N3C4) (7%)
880	899 (−176, −5)	W(C8H) (51%); W(N1H) (19%); TO(C8N7) (8%); W(N9H) (6%)
833	845 (0, +31)	W(N9H) (38%); W(C2N2) (20%); TO(N9C8) (10%); TO(C4N9) (7%); W(C8H) (7%); TO(C2N3) (6%)
799	795 (+37, −94)	W(N1H) (49%); W(C8H) (15%); TO(N1C6) (13%); TO(C2N1) (6%); W(C6O6) (5%)
646	643 (−2, −118)	W(NH2) (68%); W(N1H) (15%); TO(C2N1) (6%)
545	540 (−4, −69)	W(C6O6) (32%); TO(C2N1) (21%); TO(N1C6) (17%); TO(C2N3) (7%); TO(N3C4) (7%)
485	486 (−33, −28)	TO(N9C8) (36%); TO(C8N7) (33%); W(N1H) (8%); TO(N7C5) (6%)
391	399 (−8, −55)	W(C2N2) (30%); W(N1H) (27%); TO(C2N2) (12%); TO(C2N1) (8%); TO(C8N7) (6%)
324	325 (0, −16)	W(C6O6) (32%); W(N1H) (27%); TO(C5C6) (11%); W(N9H) (7%); TO(C2N2) (6%)
231	247 (0, −17)	TO(C2N2) (25%); TO(N1C6) (16%); W(N9H) (15%); TO(C5C6) (12%); TO(C8N7) (9%); W(C6O6) (7%); W(C2N2) (6%)
197	199 (−5, −12)	TO(N9C8) (22%); TO(C4N9) (20%); W(N1H) (15%); TO(C4C5) (10%); W(C2N2) (9%); TO(C5C6) (8%)
157	169 (−4, −11)	W(C2N2) (25%); TO(C2N2) (14%); TO(C2N1) (18%); W(N1H) (11%); TO(N7C5) (10%); TO(N3C4) (7%)
	148 (−2, −26)	TO(C2N2) (33%); TO(C2N3) (16%); TO(C2N1) (15%); W(C2N2) (12%); W(N1H) (11%)

experimental lattice spectrum (observed below 150 cm^{-1}, Fig. 6b) with itself (giving rise to the second-order lattice contribution, Fig. 6c) and with the simulated first-order molecular spectrum (Fig. 6d). The third-order NIS spectrum (Fig. 6e) was simulated by convolving the second-order lattice contribution (Fig. 6c) with the simulated first-order molecular spectrum (Fig. 6a). Each of these simulated spectra (Figs. 6a–e) has been normalized to its strongest band. The final simulated NIS spectrum (Fig. 6f) was obtained by adding these spectra, taking into

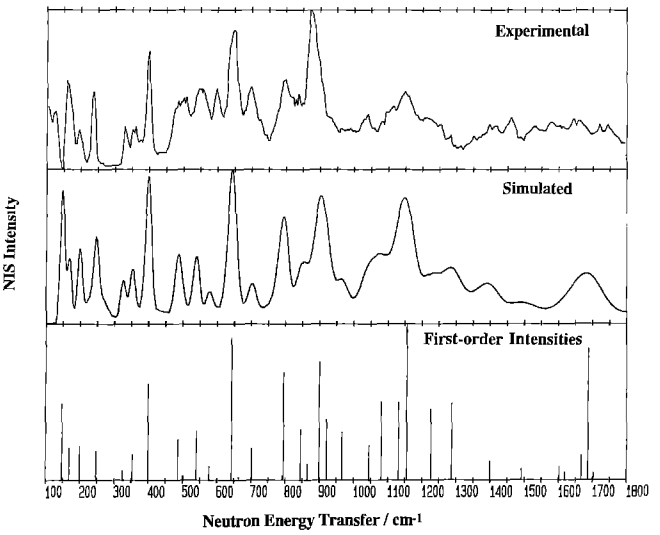

Fig. 3. Comparison of the experimental (top) and simulated (*middle*) NIS spectra for guanine in the 100–1800 cm^{-1} spectral region The vertical lines (*bottom*) represent the calculated first-order peak intensities (see text)

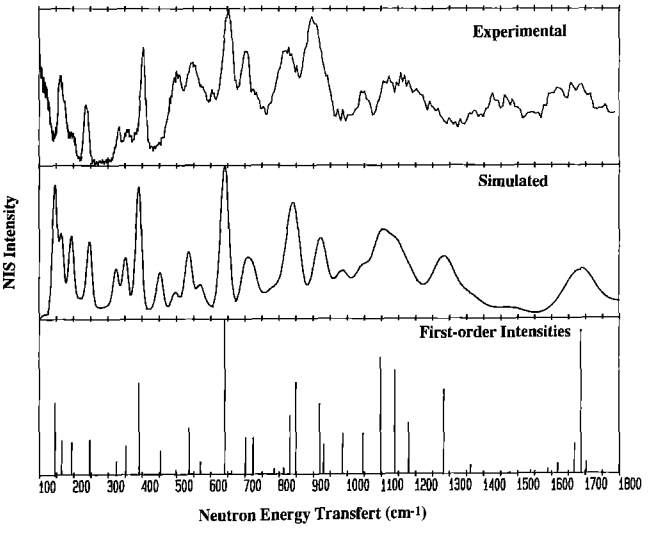

Fig. 4. Same as Fig. 2, but for G-d1

account the multiplying factors mentioned in Fig. 6. No distinct side-band (due to phonon-wings) had been added to the first-order NIS spectra (Figs. 3–5) by our multi-phonon treatment. Only a global increase in the spectral background and a little broadening of some NIS bands can be noticed. The satisfactory agreement of experimental with simulated NIS spectra leads us to conclude that the simulation containing the first- to third-order is quite sufficient for the molecules of interest: in other words, higher order (equal to or greater than 4) spectra would also contribute to a global background increase. This simulation allowed the hydrogen atom mean square amplitude to be estimated as: 0.309 $Å^2$ for the internal modes and 0.803 $Å^2$ for the external modes. In the middle part of Figs. 3–5, we have compared the final simulated NIS spectra with the experimental ones, in the spectral region above 100 cm^{-1}.

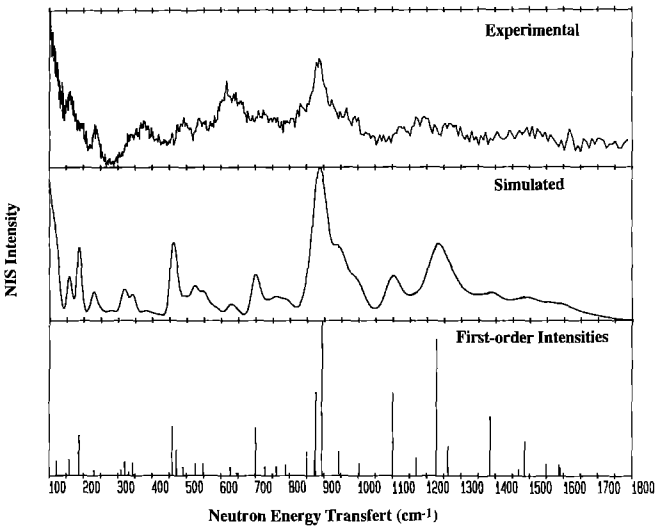

Fig. 5. Same as Fig. 2, but for G-d4

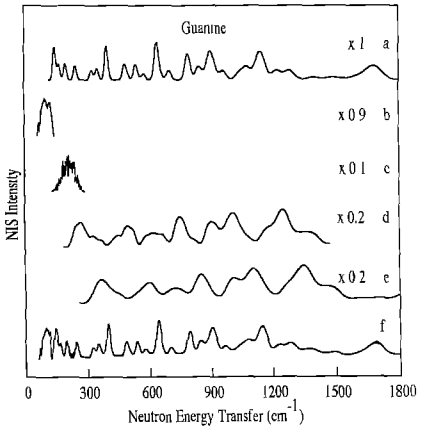

Fig. 6. Different steps of the NIS spectral simulation in the case of pure guanine. *a* First-order simulated spectrum (internal modes). *b* Lattice modes as extracted from the NIS experimental spectrum in the region below 150 cm^{-1} (see also Fig. 2a). *c* Convolution product of lattice spectrum with itself. *d* Convolution product of the first-order calculated spectrum with the lattice experimental spectrum. *e* Convolution product of the first-order calculated spectrum with the second-order lattice spectrum. *f* Final reconstituted (sum) spectrum by taking into account the multiplying factors mentioned in the right corner of the *a*–*e* spectra (see also the text, Sect. III-C)

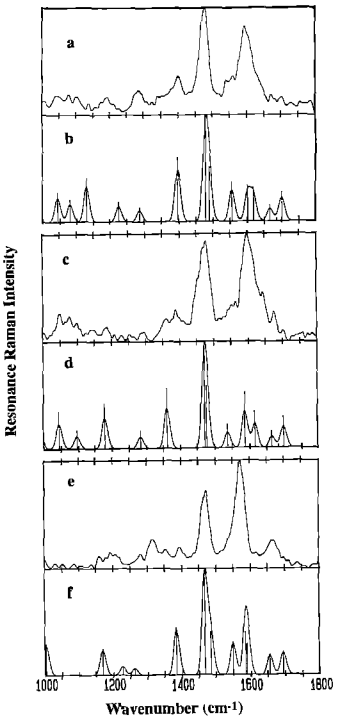

Fig. 7. Comparison of the experimental *a* and simulated *b* RRS spectra for guanine. The same kind of comparison is made for G-d1 (*c* and *d* traces), and G-d4 (*e* and *f* traces). The vertical lines represent the calculated first-order intensities (see text)

As far as the RRS intensities are concerned, the simplified theory previously employed, based on the "small shift approximation" (Blazej and Peticolas 1977; Peticolas et al. 1980), was used in considering only the electronic transition between the ground- and the first molecular excited states (which corresponds to the 257 nm excitation wavelength). This theory is only valid for the in-plane base modes involved in $\pi \rightarrow \pi^*$ transitions occurring in the base planes. As mentioned above, it uses the chemical bond-order changes induced by the proper electronic transition: here we used the bond-order changes estimated by quantum chemical calculations (Tsuboi et al. 1987). The experimental RRS spectra are compared with the simulated spectra in Fig. 7 for guanine and its deuterated species. RRS band shapes have also been simulated by Gaussian curves. A constant 20 cm^{-1} half-width has been considered for all of the simulated Raman bands. In all cases, the calculated spectrum was normalized to the experimental one (from the strongest band), allowing the relative intensities to be directly compared.

E. Normal mode graphical representation

The graphical representations of the guanine vibrational modes are presented on Figs. 8 (in-plane modes) and 9 (out-of-plane modes). For each vibrational mode, the equilibrium molecular configuration along with the most distorted geometries are presented.

IV. Discussion

In the following discussion the spectral peaks observed, their origin and their nature are discussed for three distinct spectral regions.

As shown in Tables 2 to 4, the modes located below 1000 cm^{-1} contain important contributions from the angle bending coordinates. Consequently, the RRS intensities of these modes cannot be correctly estimated by the simplified RRS theory (only valid for in-plane stretching modes) used in the pesent investigation (Blazej and Peticolas 1977; Peticolas et al. 1980; Tsuboi et al. 1987). Further corrections to this theory, accounting for the angle bending contributions to the RRS intensities, would be needed to reproduce the modes located in the spectral region below 1000 cm^{-1}. In Fig. 7, our spectral shape

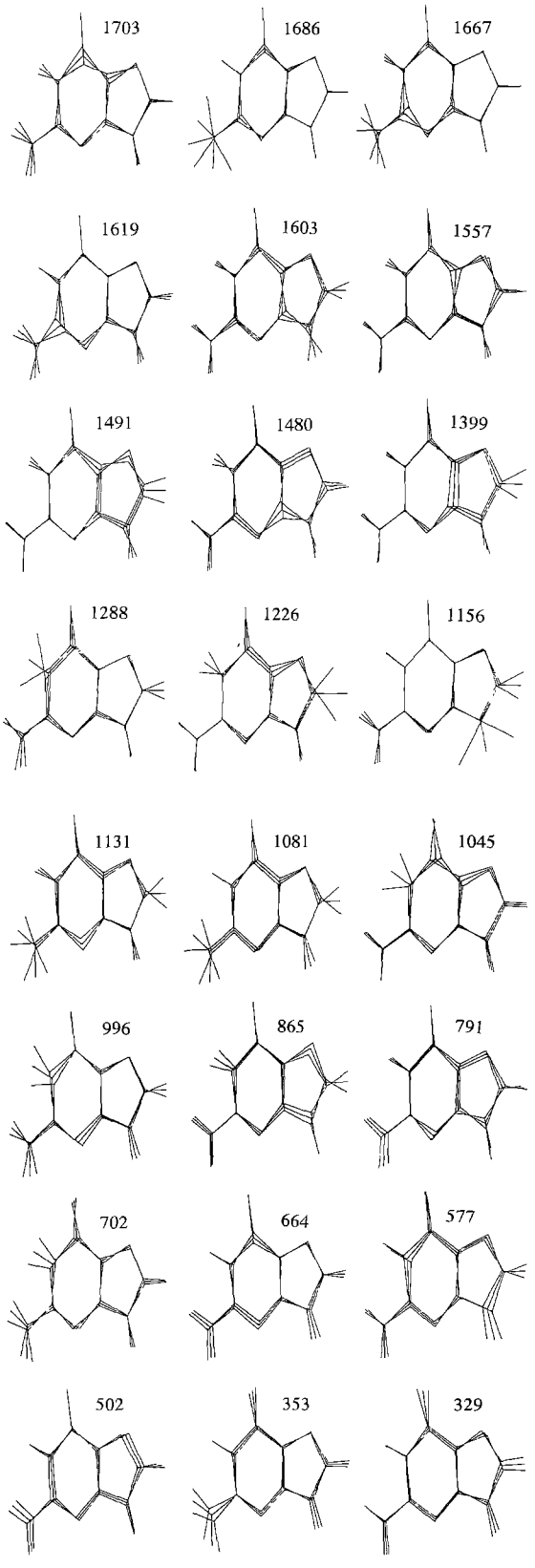

Fig. 8. Graphical representation of the calculated in-plane vibrational modes of guanine. The vibrational wavenumber (cm^{-1}) of each mode has been indicated. The assignment of these modes in terms of internal coordinates is given in Table 2

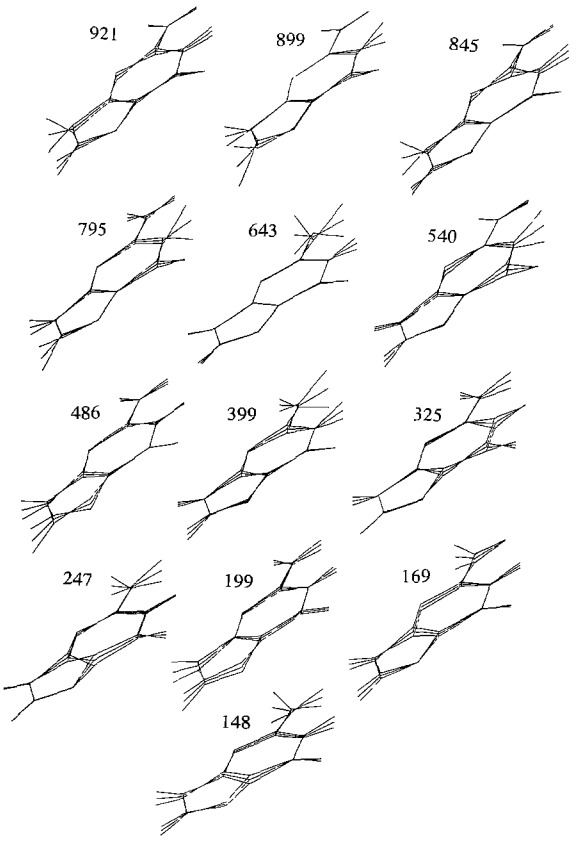

Fig. 9. Same as Fig. 8 but for the calculated out-of-plane vibrational modes. The assignment of these modes in terms of internal coordinates is given in Table 5

simulation is limited to the region above 1000 cm^{-1}, in which the in-plane vibrational modes consist mainly of the base bond-stretching motions.

A. 3500–2000 cm^{-1} spectral region

The vibrational modes located in this region arise mainly from the N–H and C–H stretching motions. The calculated wavenumbers and assignments are quite similar to those previously published (Majoube 1984) on the basis of classical Raman scattering or infrared absorption measurements.

B. 1800–1000 cm^{-1} spectral region

No out-of-plane vibrational modes are located in this spectral region. In addition, the low NIS spectral resolution in this region (Fig. 2a–c) is too poor to allow any spectral assignments to be made. In contrast, the RRS spectra (Fig. 2d–f) give rise to intense and well resolved bands, allowing the frequency shifts of the in-plane modes observed upon selective deuteration to be monitored: this is also revealed by the very good agreement between simulated and experimental data. Tables 2 to 4 show a major contribution from double-bond stretching vibrations to most of the modes located above 1400 cm^{-1}.

Our assignments for the in-plane vibrational modes calculated at 1703 and 1686 cm^{-1} are different from those proposed by Majoube (1984) in the same region. On the basis of the present calculation, the C=O stretching motion (calculated at 1703 cm^{-1}) is decoupled from the NH2-scissoring mode. This new assignment accounts for the RRS band shifts experimentally observed upon deuteration of the C2-amino group. Between 1600 and 1680 cm^{-1}, our calculation predicts three vibrational modes, while only two modes have been proposed in the previous simulations (Majoube 1984). All of these three calculated modes are needed to account for the spectral intensities in this region (Fig. 7). The intense RRS band peaking at 1475 cm^{-1} is simulated by two calculated modes located at 1491 and 1480 cm^{-1}, arising mainly from C8=N7, C4=C5 and C4−N9 stretching vibrations. The calculated shifts of these bands upon C8-deuteration are in good agreement with the experimental observations.

The vibrational mode calculated at 1399 cm^{-1}, due to the guanine ring stretching modes, well reproduces the RRS band peaking at 1400 cm^{-1}. Owing to the low solubility of guanine (see experimental section), the RRS spectral information is of rather poor quality in the 1400–1000 cm^{-1} spectral region, which makes it difficult to compare the calculated and experimental data. However, our simulation yields low intensity RRS bands in this region, whose calculated wavenumbers are in good agreement with the IR and off-resonance Raman data previously obtained by Majoube (1984) from polycrystalline samples (see Tables 2 to 4).

C. 1000–150 cm^{-1} spectral region

As mentioned in our previous first-order simulation of the guanine NIS spectrum (Coulombeau et al. 1991), as well as in the paper dealing with adenine and its deuterated species (Dhaouadi et al. 1993), the NIS intensities arise mainly from the out-of-plane vibrational modes in this spectral region. However, three NIS bands peaking at 699, 592 and 358 cm^{-1} are assignable to guanine in-plane angular bending modes (Table 2). A total of nine in-plane modes are calculated, among which is the 664 cm^{-1} mode assigned to a guanine ring-breathing motion. No observed RRS or NIS band can actually be correlated with this vibrational mode. Nevertheless, on the basis of the shifts observed upon deuteration, an off-resonance Raman band observed at 651 cm^{-1} and a 645 cm^{-1} band observed in the IR spectrum of the native species may correspond to this calculated mode (Majoube 1984). This guanine vibrational mode is worthy of mention, owing to its role as a marker band of the DNA conformation, since it is coupled with a sugar vibrational motion in the DNA double helix (Thamann et al. 1981; Ghomi et al. 1988).

Out-of-plane N−H and C−H wagging modes give rise to intense NIS bands above 600 cm^{-1} (Figs. 3–5 and Table 5). Nevertheless, they are highly coupled with torsional motions (Table 5 and Fig. 9). The intense NIS bands peaking at 880 and 833 cm^{-1} include mainly C8−H and N9−H wagging modes, while the 799 cm^{-1} band is assigned to the N1−H wagging motion. The NH2 wagging motion gives rise to an intense peak at 646 cm^{-1}. Other wagging modes related to bonds involving heavy atoms, such as C2−N2 and C6=O6, contribute to the intense NIS bands located at 545, 391 and 324 cm^{-1} (and to a shoulder on the high-wavenumber side of the 157 cm^{-1} band).

Ring torsional modes are mainly located below 500 cm^{-1}. Among them, the C2−N2 torsional mode contributes to the intense NIS bands peaking at 231 and 157 cm^{-1}. The latter band also includes ring torsional motions and can be considered as the lowest wavenumber mode of the internal vibrations of guanine.

V. Conclusion

Molecules such as the nucleic acid bases are of low point symmetry. Consequently, their vibrational analysis becomes difficult since the number of force constants in a general valence force field far exceeds the number of measured wavenumbers. Thus, several force fields can easily be obtained so as to reproduce reasonably well all of the observed vibrational wavenumbers. However, these force fields may be quite different from each other and give rise to different nuclear displacements. In the present paper, our aim was to obtain a consistent force field which reproduces simultaneously the RRS and NIS wavenumbers and intensities. It should be underlined that the NIS technique is a powerful method which allows valuable information on the nuclear displacements to be obtained. In addition the RRS intensities can be directly related to vibrational normal coordinates. Thus, all of the information obtainable from normal coordinate analysis (vibrational wavenumbers, atomic displacement amplitudes) can be tested by the combination of these two techniques. Moreover, the complementary aspects of the RRS and NIS techniques should be mentioned, as regards the spectral regions and the nature of the vibrational modes explored by each method. The present investigation leads to a better understanding of all of the molecular vibrational motions in the 150 to 1800 cm^{-1} range. In addition, the reliability of the molecular force field is justified by its ability to reproduce the frequency shifts experimentally observed upon selective deuteration. The present force field proposed for guanine, as well as that previously proposed for adenine (Dhaouadi et al. 1993), constitute a complete basis for studying the purine base vibrational modes. The transferability of this force field to modified purine compounds, such as 2-aminoadenine and hypoxanthine, has been successfully tested by us (unpublished results). The same approach can also be extended to the case of pyrimidine bases. Finally, this reliable force field, which accounts for the low- and high-wavenumber vibrations, can be employed in future studies on molecular mechanics and dynamics.

Acknowledgements. The authors would like to thank Dr. J. Tomkinson and the Rutherford Appleton Laboratory staff for their technical assistance in using the TFXA and ISIS facilities to obtain the NIS spectra of guanine and its deuterated species. During his stay at the Institut Curie, P. Mojzes was funded by the French Foreign Office within the framework of the MICECO program.

References

Blazej DC, Peticolas WL (1977) Ultraviolet resonant Raman spectroscopy of nucleic acid components. Proc Natl Acad Sci, USA 74:2639–2643

Brunel Y, Coulombeau C, Coulombeau Ce, Jobic H (1985) Optical and neutron inelastic scattering study of 2,3-methylnobornanes. J Phys Chem 89:937–943

Coulombeau C, Dhaouadi Z, Ghomi M, Jobic H, Tomkinson J (1991) Vibrational mode analysis of guanine by neutron inelastic scattering. Eur Biophys J 19:323–326

Delabar JM, Majoube M (1978) Infrared and Raman spectroscopic study of ^{15}N and D substituted guanines. Spectrochim Acta 34A:129–140

Dhaouadi Z, Ghomi M, Austin JC, Girling RB, Hester RE, Mojzes P, Chinsky L, Turpin PY, Coulombeau C, Jobic H (1993) Vibrational motions of bases of nucleic acids of as revealed by neutron inelastic scattering and resonance Raman spectroscopy. 1. Adenine and its deuterated species. J Phys Chem 97:1074–1084

Ghomi M, Letellier R, Taillandier E (1988) A critical review of nucleosidic vibration modes appearing in the 800–500 cm^{-1} spectral region, based on new harmonic dynamics calculations. Biopolymers 27:605–616

Gusoni M, Zerbi G (1968) Symmetry coordinates in molecular vibrations. J Mol Spectrosc 26:485–488

Jobic H, Lauter HJ (1988) Calculation of the effect of the Debye-Waller on the intensities of molecular modes measured by inelastic scattering. Application to hexamethylenetetramine. J Chem Phys 88:5450–5456

Majoube M (1984) Vibrational spectra of guanine. A normal coordinate analysis. J Chim Phys (Paris) 81:303–315

Penfold J, Tomkinson J (1988) The ISIS time focussed crystal analyser spectrometer, TFXA. Rutherford Appleton Laboratory Report (Chilton) RAL-86-019

Peticolas WL, Strommen DP, Lakshminarayanan V (1980) The use of resonant Raman intensities in refining molecular force fields for Wilson G-F calculations and obtaining excited state molecular geometries. J Chem Phys 73:4185–4191

Thamann TJ, Lord RC, Wang AHJ, Rich A (1981) The high salt form of poly d(G–C). poly d(G–C) is left-handed Z-DNA: Raman spectra of crystal and solutions. Nucl Acids Res 9:5443–5457

Tsuboi M, Nishimura Y, Hirakawa AY, Peticolas WL (1987) Resonance Raman spectroscopy and normal modes of the nucleic acide bases. In: Spiro TG (ed) Biological applications of Raman spectroscopy, vol 2. Wiley, New York, pp 109–179

Wilson EB, Decius JC, Cross PC (1955) Molecular vibrations. McGraw Hill, New York